RSC Advances

ROYAL SOCIETY OF CHEMISTRY

www.rsc.org/advances

Investigation on corrosion protection and mechanical performances of minerals substituted hydroxyapatite coating on HELCDEB treated titanium using pulsed electrodeposition method

D. Gopi [a,b,*], A. Karthika[a], D. Rajeswari[a,c], L. Kavitha[c], R Pramod[d], Jishnu Dwivedi[d]

[a]*Department of Chemistry, Periyar University, Salem 636011, India*
[b]*Centre for Nanoscience and Nanotechnology, Periyar University, Salem 636011, India*
[c]*Department of Physics, School of Basic and Applied Sciences, Central University of Tamilnadu, Thiruvarur 610101, India*
[d]*Industrial and Medical Accelerator Section, Raja Ramanna Centre for Advanced Technology, Indore 452013, India*

* Corresponding author. Tel.: +91 427 2345766; fax: +91 427 2345124.
E–mail address: dhanaraj_gopi@yahoo.com (D. Gopi).

Abstract

The present work is aimed for the investigation on the effects of minerals (strontium, magnesium and zinc) substituted hydroxyapatite (M–HAP) coating on high energy low current DC electron beam (HELCDEB) treated titanium (Ti). The M–HAP coating obtained over the untreated and HELCDEB treated Ti by pulsed electrodeposition method was characterized by scanning electron microscopy (SEM), X–ray diffraction (XRD), Fourier transform infrared spectroscopy (FT–IR), Raman spectroscopy, X-ray photoelectron spectroscopy (XPS) and electrochemical techniques. The M–HAP coating was achieved on 500 keV and 700 keV treated Ti. The coating on 700 keV HELCDEB energy electron beam treated Ti showed better corrosion resistance property than the coating obtained on 500 keV HELCDEB treated and untreated Ti. The M–HAP coating on HELCDEB treated Ti showing typical flower–like morphology, exhibited better resistance to corrosion in simulated body fluid (SBF), along with the increased microhardness and decreased contact angle. The *in vitro* study of the coating was conducted by immersing them in the SBF solution for the period of 1–7 days. All the results clearly evidenced that the M–HAP coating on 700 keV HELCDEB treated Ti could enhance the corrosion

resistivity with improved mechanical properties, which finds its major role in orthopedic field by improving the implant fixation with human bone.

1. Introduction

The development of biocompatible implant material is the most imperative research area in medical science. Metallic implants such as Ti and its alloys have gained significant attention in the field of orthopedic and dental prostheses. However due to their bioinertness,[1] the contact between them and bone tissues is just a sort of mechanically embedded connection and their direct implantation into the human body will also cause a lot of problems including low strength of bone combination, poor bioactivity, long curing time and metallic ions migrating towards the body in physiological environments.[2] Hence, metallic implants are coated with osteoconductive bioceramics especially HAP [$Ca_{10}(PO_4)_6(OH)_2$]. The HAP can develop a tight bonding with bone tissue which is stable towards bioresorption and has no adverse effects on the human organism.[3] The natural HAP present in bone contains different elements that have proven to play a key role in bone formation and normal functions of bone tissue. Hence the synthetic HAP has flexibility to accept metal ions substitution and the small quantity of these ions improves the quality of clinical applications. Among many mineral ions,[4,5] strontium (Sr), magnesium (Mg) and zinc (Zn) have recently attracted the upcoming young scientists.

Sr is an important trace element in human body and low dose of Sr diminish the risk fractures in postmenopausal osteoporotic patients.[6] While promoting bone formation, Sr favors bone healing[7,8] where Sr has been shown to enhance preosteoblasts proliferation and decrease bone resorption by inhibiting the osteoclast resorbing activity and osteoclastic differentiation.[8] Numerous reports stated that the effects of Sr–HAP have tended to enhance their bioactivity and

biocompatibility by the release of Sr^{2+} ions,[9–11] and also found to enhance the mechanical properties.[12]

Similarly, Mg is essential for bone metabolism since the depletion of Mg adversely affects skeletal metabolism and cause cessation of bone growth.[13,14] Mg is the fourth most abundant cation in the human body and is recommended to interact with integrins of osteoblasts, which are responsible for cell adhesion and stability.[15,16] Zn occurs naturally in human bone and has functions in enzyme regulation, cell division and bone formation, which is strongly associated with the growth, development, and maintenance of healthy bones.[17] Also Zn has antibacterial activity, thus it minimizes the bacterial load on the implant surface after orthopedic implantation[18] and improves the mechanical strength.[19] Bone growth impediment and defects are the common findings in humans and animals due to Zn deficiency.[20,21] Zinc has been reported to have a stimulatory effect on bone formation and mineralization. [22] Recently, our research group has reported the synthesis of minerals (Sr, Mg and Zn) substituted HAP with improved bioactivity [23] and also the development of Sr, Mg substituted HAP coating on polymer protected 316L SS for improved biocompatibility.[24] In addition, Gopi et al. reported the development of CNT/CMC/M-HAP composite and its biological activity on HOS MG63 osteoblast cells.[25] Furthermore, Aina et al. investigated the effect of Sr, Mg ions addition in HAP structure on its physico-chemical properties[26] and Cox et al. studied live/dead assay using the MC3T3 osteoblast precursor cells against the as-synthesized Sr, Mg, and Zn substituted HAP.[27]

The important requirement of a bioceramic coating is its good adhesion to the implant material. In order to obtain an adhesive coating with enhanced corrosion resistance, and to achieve better osseointegrated implant the surface of the titanium is mainly modified. This can induce a new bone growth onto the implant.

The surface properties of bioimplant materials, such as surface roughness and wettability, play an essential role in bonding with the living cells.[28] Many surface modification techniques are used to modify the surface of implants viz., chemical etching, alkaline heat treatment, laser irradiation, microwave, electron beam, plasma and ion beam irradiation/implantation.[29] In particular, the electron beam treatment has been proven to be an efficient method for surface modification of the metallic materials.[30] The energetic electron beam treatments promote the microhardness and corrosion resistance of the implants. Dong et al.,[29] and Proskurovsky et al.,[31] have reported that the pulsed electron beam treatment improved the physical, chemical and mechanical properties of the metal which may arise due to the metastable states in the surface layers of the metal. This technique has several advantages like impeding the surface of implant from oxidation, forming strong bond between the substrate and melted surface, and preventing the surface of the implant from cracks and pores [32]. Recently Gopi et al.,[32,33] has developed the HAP and Sr–HAP coating with flower–like morphology on HELCDEB treated Ti and 316L SS by pulsed electrodeposition and electrodeposition, respectively. In HELCDEB irradiation, the surface undergoes superfast heating, melting and solidification to provide improved physicochemical properties and bonding strength to the material which are unachievable with other surface treatments[33].

Many methods were developed to obtain bioactive pure and substituted HAP coatings such as biomimetic,[34,35] pulsed laser deposition,[36] electrochemical deposition,[37–40] micro arc oxidation,[41] plasma spraying,[42] etc. In which, the electrodeposition can be used to deposit HAP on any complex geometry substrates. But, in this method, H_2O is reduced to OH^- and along with this large amount of H_2 is produced. The H_2 gas severely prevents the nucleation and growth of HAP on the metallic surface, which results a loose, porous and low adhesive coating.[43] However,

pulsed electrodeposition has advantages like higher deposition rate, control of deposition composition, improved coating quality with desired structure, and regulation of the coating thickness. In pulsed electrodeposition process, hydrogen peroxide (H_2O_2) inclusion in the electrolyte restricts the H_2 bubbles evolution, which enhances the ionic mobility and paves the way for the deposition of mineral ion on the implant material.[44, 45]

The present work aims to study the effect of M–HAP coating obtained on the HELCDEB treated Ti at different irradiation conditions. The corrosion resistive performance and mechanical properties of the M–HAP coating on HELCDEB treated Ti were evaluated. Along with this, the *in vitro* dissolution study of the M–HAP coating was verified in the simulated body fluid (SBF) environment in order study the reactivity and reliability of the M–HAP coating.

2. Experimental

2.1. Preparation of Ti Substrate

The pure Ti metals (99.99 %) with a size of 10×10×3 mm were used as the substrate for the pulsed electrodeposition. These substrates were abraded using 400–1200 silicon carbide grit sheets and subsequently polished with 1.5 μm diamond paste. In between and after the polishing process, the substrates were washed and ultrasonically cleaned with acetone to prevent the cross contamination of abrasive particles.

2.2. High Energy Low Current Dc Electron Beam Treatment on Ti

The specimens were surface treated using 700 keV DC accelerator with electron beam of 1.5 mA current at 500 keV and 700 keV energies to enhance the mechanical properties and corrosion resistance of the Ti metal. The procedure for the irradiation was followed as per our previous report.[33]

2.3. Preparation and Pulsed Electrodeposition of M–HAP

Analytical grade 0.294 M $Ca(NO_3)_2.2H_2O$, 0.042 M $Sr(NO_3)_2.6H_2O$, 0.042 M $Mg(NO_3)_2.6H_2O$ and 0.042 M $Zn(NO_3)_2$ were dissolved in deionized water, respectively and 0.25 M $(NH_4)_2HPO_4$ was dissolved separately. Then, the phosphate ion solution was added drop wise into the cationic solution by keeping the target ratio of (Ca+Sr+Mg+Zn)/P as 1.67. The electrolyte was de–aerated with N_2 for 30 min and pH of the electrolyte was adjusted to 4.5 using NH_4OH. The electrolyte temperature was maintained at 65 °C using thermostat and the magnetic stirrer was used to sustain the uniform concentration of the electrolyte at a speed of 180 rpm. Prior to start the coating procedure, hydrogen peroxide (2000 ppm) was added to the electrolyte solution in order to diminish the hydrogen gas evolution.[33]

The pulsed electrodeposition was carried out in a regular three electrode system using an electrochemical workstation (CHI 760C (CH Instruments, USA)) in which the untreated Ti, HELCDEB treated Ti specimens and M–HAP coating on HELCDEB treated Ti specimens act as working electrode, respectively, whereas the platinum electrode and saturated calomel electrode (SCE) act as counter and reference electrodes, respectively. The deposition was performed for 1 h on untreated and surface irradiated Ti samples in a galvanostatic mode with a constant current density of 1.0 mA cm^{-2}. The pulse on and off time was kept constant as per our previous study,[33] the optimum condition of 1 s pulse on time and 4 s pulse off time with respect to the current density of 1.0 mA cm^{-2} and 0 mA cm^{-2}. After the coating process, the specimens were removed from the electrolyte and washed with deionized water, then stored in a desiccator for 4 h to dry the samples.

2.4. Structural Characterizations

The FT–IR spectra were obtained using a Perkin Elmer RX1 FT–IR spectrometer and were recorded in the 4000–400 cm^{-1} region with 4 cm^{-1} resolution by using KBr pellet technique. The Raman spectra of M-HAP coatings were obtained with a Raman Spectrometer (Horiba-Jobin, LabRAM HR) with the scan range of 50–3000 cm^{-1}. All the spectra were recorded at ambient temperature.

The X–ray diffraction (XRD) patterns of the pure Ti, pure HAP and as–coated samples were obtained using PANalytical X'Pert PRO diffractometer in the range between $20° \leq 2\theta \leq 70°$ with Cu Kα radiation (1.5406 Å).

The surface morphology and actual composition of the as–deposited samples were observed by a high resolution scanning electron microscopy (HRSEM, JSM 840A Scanning microscope, JEOL–Japan) equipped with energy dispersive X–ray analysis (EDAX). The cross-sectional SEM analysis of all the coated samples was also carried out using HRSEM. The average thickness of each coating was obtained from 3 measurements at different positions.

X-ray photoelectron spectroscopy (XPS; Omicron Nano- Technology instrument) with a focused monochromatic Al Kα source (1486.6 eV) for excitation was utilized for chemical composition analysis of M-HAP coating. The electron take off angle was 54.7° and the XPS survey spectrum over a binding energy range of 0-1100 eV was acquired with analyzer pass energy of 50 and 20 eV for high-resolution elemental scans. The vacuum pressure was around 3.5×10^{-10} mbar during spectral acquisition. Data analysis was carried out with EIS-Sphera software provided by the manufacturer.[25]

2.5. Contact Angle Measurements

The contact angle measurement of the untreated, 500 keV and 700 keV HELCDEB treated Ti specimens were analyzed using a video–based contact angle meter (OCA 15EC, Data Physics Instruments, Germany). An equal volume of distilled water was placed on every sample by means of a micropipette, forming a drop or spreading on the surface. Photos were taken through to record the shape of the drops and the contact angle was measured. Five measurements were taken at different locations on each specimen and an average contact angle was calculated.

2.5. Mechanical properties of the M–HAP coating

2.5.1. Adhesion strength

The adhesion strength of M–HAP coatings on untreated, 500 keV and 700 keV HELCDEB treated Ti was evaluated by pull–out test according to the American Society for Testing Materials (ASTM) international standard F1044–05[46] with five experiments for each sample carried out. The specimens were subjected to tests at a constant cross–head speed using a universal testing machine (Model 5569, Instron).

2.5.2. Vickers hardness test

The surface Vickers micro hardness was measured at the top surface of the untreated, HELCDEB treated, M–HAP coatings on the untreated and HELCDEB treated Ti samples to obtain the relevant statistics. The hardness value is an average of 8 different hardness test measurements.

2.6. Electrochemical Characterizations

The potentiodynamic polarization study was performed for the untreated, HELCDEB treated and M–HAP coatings on the untreated and HELCDEB treated Ti samples using the electrochemical workstation (CHI 760C, USA) in SBF solution. These Ti samples with an

exposed surface area of 1 cm^2 were used as the working electrode. The SBF solution was prepared by maintaining pH at 7.4 and the temperature was kept at 37 °C.[47] Potentiodynamic polarization studies were performed in a potential range of –1 to 1 V at a scan rate of 0.001 V s^{-1}. The potentiodynamic polarization was repeated at least three times in order to obtain the average test results.

2.7. Inductively Coupled Plasma Atomic Emission Spectroscopy

The SBF dissolution study on M–HAP coating was performed by inductively coupled plasma atomic emission spectroscopy (ICP–AES, Thermo Electron IRIS INTREPID II XSP DUO, USA). The fresh SBF was maintained by contacting the coated specimen for 1 day, 4 days and 7 days.

3. Results and discussion

3.1. Functional Group Analysis

The FT–IR spectra of the M–HAP coating on untreated Ti, and 500 keV and 700 keV HELCDEB treated Ti are given in Fig. 1(a–c). The observed characteristic peaks at 480.89 (υ_2), 563.00 and 601.34 (υ_4), 977.89 (υ_1), 1028.75 and 1098.26 (υ_3) cm^{-1} correspond to the PO_3^{4-} group. The peaks at 3427.87 and 1642.93 cm^{-1} were assigned to the stretching and bending mode of the adsorbed water. Moreover, the characteristic –OH peaks of HAP at around 3569.41 cm^{-1} and 633.12 cm^{-1} are due to the stretching and bending modes.[48] Thus, the FT–IR spectra confirmed the formation of M–HAP coating by the pulsed electrodeposition and no other impurities were identified.

The Raman spectra of the M-HAP coatings that contain bands due to each of the four phosphate internal vibration modes are shown in Fig 2 (a and b). The bands due to the stretching and librational modes of the hydroxyl ions are weak and provide little information on the mineral

environment in the Raman spectrum.[49] Therefore, the interest was focused on the phosphate modes. The most intense bands at 964 cm^{-1} are due to the symmetric υ_1 (PO_4) stretching mode of the 'free' tetrahedral phosphate ion. The υ_1 (PO_4), υ_2 (PO_4) bands at 447, 432 cm^{-1}, υ_3 (PO_4) bands at 1082, 1073, 1047, 1026 cm^{-1} and υ_4 (PO_4) bands at 611, 603, 587 cm^{-1} were determined (Fig 2 (a and b)). The Raman spectra of M-HAP coating demonstrate the typical stretching frequency of phosphate ion which confirms the presence of calcium phosphate phase. No other additional bands were observed and this confirms the absence of impurities which is correlated with FT-IR results.

3.2. Diffraction Studies

The XRD patterns of Ti substrate, pure HAP coating on untreated Ti and M–HAP coating on untreated Ti, and 500 keV and 700 keV HELCDEB treated Ti are shown in Fig. 3(a–e). The XRD pattern of pure Ti showed no diffraction peaks apart from Ti peak (Fig. 3a). The pattern in Fig. 3(c) is less intense and experienced a slight shift when compared to that of pure HAP (Fig. 3b) which is well agreement with ICDD No. 09–0432.[33] In this regard, the main diffraction peaks of HAP obtained at 25.9°, 31.7°, 32.2° and 32.9° are shifted to the left side due to the substitution of mineral ions which occurred by expansion and contraction in the HAP lattices [26,50,51]. Figure 3(d and e), shows the intense peaks for the M–HAP coating obtained on 500 keV and 700 keV HELCDEB treated Ti which evidenced that the crystallinity of the coating is high. These patterns reveal the presence of Sr, Mg and Zn in the M–HAP coating.[48]

3.3. Morphological Studies

The SEM images of the untreated, 500 keV and 700 keV electron beam treated Ti, M–HAP coatings on the Ti metal before and after HELCDEB treatments are displayed in Fig. 4(a–f). The morphology of the polished Ti is displayed in Fig. 4a. The M–HAP coating on

the untreated Ti exhibits sphere–like morphology at 1 s pulse on time and 4 s pulse off time and is shown in Fig. 4b. The modified surface of the 500 keV and 700 keV HELCDEB treated Ti specimens are shown in Fig. 4(d and g), respectively, and are consisting of the homogeneous micro–structured eruptions formed during the rapid solidification of the surface melted layer. The magnified views of the surface treated Ti are given as insets in Fig. 4(d and g). An uniformly arranged flower–like coating (Fig. 4e) which covers the entire surface was obtained for 500 keV HELCDEB treated Ti substrate. The exact flower–like structure might have been originated from the centre of the erupted spot, having diameter of few micrometers (~8 μm) as displayed in Fig. 4e as inset. The Fig. 4h also showed the formation of flower–like M–HAP coating over the 700 keV HELCDEB treated Ti. The magnified image also showed flower-like structure, which is evidenced as inset in Fig. 4h. Hence, from the morphological studies, it is clearly evident that the surface treatment played a prime role in the formation and uniformity of flower–like structured M–HAP coating. The Fig. 4(c, f and i) display the cross-sectional view of the as-developed coatings. The thickness of the M-HAP coating on untreated Ti (Fig. 3c), 500 keV HELCDEB treated Ti (Fig. 3f) and 700 keV HELCDEB treated Ti (Fig. 3i) were ranged from 27-29 μm.

The Fig. 4j shows the EDAX spectrum of M–HAP coating on the HELCDEB treated Ti. The distribution of Sr, Mg, Zn, Ca, P and O ions is evidenced in Fig. 4j and this study supports the presence of the mineral ions on the surface treated Ti. Also, the quantitative measurement of M–HAP coating is shown as inset in Fig. 4j.

3.4 X-ray photoelectron spectroscopic study

XPS is a significant surface analytical technique which is useful for the detection of elements present in a material. The XPS survey spectrum of M-HAP coating on 700 keV treated

Ti is shown in Fig. 5. The survey spectrum identified Ca, P, Sr, Mg, Zn, and O as the major constituents of the M-HAP coating on 700 keV HELCDEB treated Ti substrate. The observed peak positions near 347.5 and 350.7 eV are attributed to $Ca2p_{3/2}$ and $Ca2p_{1/2}$, respectively.[52] The binding energy of P2s is 190.2 eV and the peak at 133.2 eV is an overlap of Sr3d and P2p because of the $Sr3d_{5/2}$ (133 ± 0.5 eV), moreover the P2p (132-133 eV) lines were closely located to the Sr peak.[53] The peak of O1s observed with binding energy of 530.8 and 532.2 eV are attributed to oxygen associated with phosphate group and absorbed water in the M-HAP, respectively.[54] The peak at 49.9 eV is detected for Mg and the typical binding energy of Zn2p is 1022.0 eV.[55] So the XPS data clearly indicates the presence of minerals which confirms the M-HAP formation.[25]

3.5. Contact Angle Measurements

The contact angle between the deionized water and 500 keV HELCDEB treated Ti showed 53.09° whereas for 700 keV HELCDEB treated Ti, it was 49.05° (Fig. 6b and 6c). When compared to that of untreated Ti (75.70°), these contact angles suggested that the hydrophobic surface turns into hydrophilic.

3.6. Adhesion Strength

Figure 7 summarizes the adhesion strength of the M–HAP coating on untreated Ti, M–HAP coating on 500 keV and 700 keV HELCDEB treated Ti. The adhesion strength of the M–HAP coating on untreated Ti was measured as 20.4±1.3 MPa. The M–HAP coating on 700 keV HELCDEB treated Ti exhibits slightly higher adhesion strength (22.1±1.1 MPa) than that of the coating obtained on 500 keV energy treated Ti (21.6±0.7 MPa). These results fulfill the main requirement of the coating for the prolonged life of the implant.

3.7. Vickers Microhardness

The results of the microhardness for the M–HAP coatings on untreated Ti, and M–HAP coatings on Ti which was surface treated with 500 and 700 keV electron beams, respectively are shown in Fig. 8. The microhardness increases for the M–HAP coating on HELCDEB treated Ti samples in comparison with the coating on untreated Ti (6.31±0.42 GPa). The M–HAP coating on 700 keV treated Ti sample (7.16±0.6 GPa) exhibits slightly higher hardness value than the sample at 500 keV (7.02±0.35 GPa). This indicates that the as–formed coating owned intact contact with the HELCDEB treated Ti substrate.

3.8. Potentiodynamic Polarization Studies

Representative potentiodynamic polarization curves of the untreated, 500 and 700 keV HELCDEB treated Ti, M–HAP coatings on untreated Ti, and M–HAP coatings on 500 and 700 keV treated Ti are shown in Fig. 9. The values of E_{corr} and I_{corr} for the untreated Ti was −0.57 V and 0.54 μA cm^{-2}, respectively and for the 500 keV treated Ti and 700 keV treated Ti were found to be E_{corr} = −0.148 V and i_{corr} =0.09 μA $cm^{-2}$and E_{corr} = −0.09 V and i_{corr} = 0.08 μA cm^{-2}, respectively. The surface treated samples showed higher E_{corr} and I_{corr} values than the untreated Ti sample. For the samples coated with M–HAP, the E_{corr} values were found to be –0.023, 0.088, and 0.245 V, while the corresponding I_{corr} values were 0.42, 0.34, and 0.22 μA cm^{-2}, respectively. The E_{corr} values for the coated samples show higher value than that of the untreated Ti sample, which indicates the passive nature of the coatings. When compared with the M–HAP coating on untreated Ti, the E_{corr} and I_{corr} values of the M–HAP coating on HELCDEB treated Ti specimens showed better shift towards the nobler direction. Particularly, the M–HAP coating on 700 keV HELCDEB treated Ti illustrated better positive shift than the M–HAP coated 500 keV HELCDEB treated Ti.

3.9. SBF Dissolution Study

ICP analysis showed that the dissolution of mineral ions occurred from of the M–HAP coating for the first day. The average Ca ion concentration in the solution improved rapidly from ~1.2 ppm to ~26.9 ppm (which is the difference between the control value and leach out value) as the immersion time increased from 0 to 1 day. Likewise, the release of Sr, Mg, Zn and P ions in the solution slightly increased as shown in Fig. 10. However, the concentration of ions release slightly decreased after 4 and 7 days. This situation indicated that up to 1 day of immersion, the dissolution of coating occurred and after that HAP deposition took place on the surface of the M–HAP coating.[56]

4. Conclusions

In this study Sr, Mg and Zn substituted HAP coating was obtained on HELCDEB treated Ti by pulsed electrodeposition method. The results are summarized as follows:

1. The presence of functional groups in the M-HAP was confirmed by FT-IR and Raman results and the influence of Sr, Mg and Zn substitution on the M-HAP was confirmed by XRD studies.
2. The SEM study exhibited typical flower-like morphology having diameter of approximately few micrometers (~8 μm) on the HELCDEB treated Ti samples. The EDAX and XPS studies revealed the presence of mineral ions (Sr, Mg, Zn, Ca, P and O) in the resultant coating.
3. The M-HAP coating on 700 keV HELCDEB treated Ti possesses higher adhesion strength than the other coatings such as M-HAP coating on 500 keV HELECDEB treated Ti and untreated Ti.

4. The electrochemical results revealed that the M–HAP coating on 700 keV HELCDEB treated Ti is showing higher corrosion protection when compared with the untreated Ti, and other coatings.
5. The ICP–AES results evidenced that no large scale dissolution occurred from the M–HAP coating in the SBF environment for 7 days, which proved the stability of the coating.

On the whole, the resultant HELCDEB treatment on Ti enhances the corrosion and mechanical properties by M–HAP coating and can be utilized in the orthopedic fields. The biological studies of the resultant coating will be published later.

Acknowledgments

One of the authors D. Gopi acknowledges the major financial support from the Department of Science and Technology, New Delhi, India (DST) and Council of Scientific and Industrial Research, New Delhi, India (CSIR) in the form of major research projects. D. Gopi and L. Kavitha also acknowledge UGC, New Delhi, India for the Research Award (Ref. No. F. 30-1/2013(SA-II)/RA-2012-14-NEW-SC-TAM-3240 and F. 30-1/2013(SA-II)/RA-2012-14-NEW-GE-TAM-3228) (2012-2014), respectively.

References

1 J. Cizek, K. A. Khor and Z. Prochazka, *Mater. Sci. Eng. C,* 2007**,** ***27***, 340.

2 A. Letic–Gavrilovic, R. Scandurra and K. Abe, *Dent. Mater. J.,* 2000, ***19***, 99.

3 C. G. Ambrose and T. O. Clanton, *Ann. Biomed. Eng.,* 2004, **32**, 171.

4 M. Vallet–Regi and J. M. Gonzalez–Calbet, *Prog. Solid State Chem.,* 2004, **41**, 3130.

5 S. V. Dorozhkin and M. Epple, *Angew Chem. Int. Ed.,* 2002, **41**, 1.

6 J. Yan, J. Sun, P.K. Chu, Y. Han and Y. Zhang, *J. Biomed. Mater. Res. Part A,* 2013, **101**, 2465.

7 E. Canalis, M. Hott, P. Deloffre, Y. Tsouderos and P. J. Marie, *Bone*, 1996, **18**, 517.

8 E. Bonnelye, A. Chabadel, F. Saltel and P. Jurdic, *Bone,* 2008, **42**,129.

9 K. K. Johal, G. M. Suarez and J. I. E. Garcia, *J. Mater. Sci. Mater. Med.,* 2002, **13**, 375.

10 S. Pina, P. M. Torres, F. G. Neunhoeffer, J. Neubauer and J. M. F. Ferreira, *Acta Biomater.,* 2010, **6**, 928.

11 E. Buache, F. Velard, E. Bauden, C. Guillaume, E. Jallot, J. M. Nedelec, D. L. Maquin and P. Laquerriere, *Acta Biomater.,* 2012, **8**, 3113.

12 N. D. Ravi, R. Balu, and T. S. Sampath Kumar, *J. Am. Ceram. Soc.,* 2012, **95**, 2700.

13 S. Wallach, Magnes. *Trace Elem.,* 1990, **9**, 1.

14 J. E. Sojka and C. M. Weaver, *Nutr. Rev.,* 1995, **53**, 71.

15 H. Zreiqat, C. R. Howlett, A. Zannettino, P. Evans, G. S. Tanzil, C. Knabe and M. Shakibaei, *J. Biomed. Mater. Res.,* 2002, **62**, 175.

16 M. Okazaki, Y. Yamasaki, Y. Yoshida, A. Shimazu, T. Uchida, T. Kubo, Y. Akagawa, Y. Hamada, J. Takahashi and N. Matsuura, *J. Biomed. Mater. Res.,* 2002, **62**, 99.

17 Y. Tang, H. F. Chappell, M. T. Dove, R. J. Reeder and Y. J. Lee, *Biomaterials,* 2009, **30**, 2864.

18 V. Stanic, S. Dimitrijevi, J. A. Stankovic, M. Mitri, B. Joki, I. B. Plecas and S. Raicevi, *Appl. Surf. Sci.,* 2010, **256**, 6083.

19 S. Sutha, G. Karunakaran and V. Rajendran, *Ceram. Int.,* 2013, **39**, 5205.

20 H. S. Hsieh and J. M. Navia, *J. Nutr.,* 1980, **110**, 1581.

21 J. T. Kim, S. H. Baek, S. H. Lee, E. K. Park, E. C. Kim, I. S. Kwun and H. I. Shin, *J. Med. Food,* 2009, **12**, 118.

22 M. Yamaguchi, *J. Trace Elem. Exp. Med.,* 1998, **11**, 119.

23 D. Gopi, S. Nithiya, E. Shinyjoy and L. Kavitha, *Spectrochim. Acta Part A,* 2012, **92**, 194.

24 D. Gopi, S. Ramya, D. Rajeswari, M. Surendiran, L. Kavitha, *Colloids Surf. B,* 2014, 114, 234.

25 D. Gopi, S. Nithiya, E. Shinyjoy, D. Rajeswari and L. Kavitha, *Ind. Eng. Chem. Res.,* 2014, **53**, 7660.

26 V. Aina, G. Lusvardi, B. Annaz, I. R. Gibson, F. E. Imrie, G. Malavasi, L. Menabue, G. Cerrato and G. Martra, *J. Mater. Sci.: Mater. Med.,* 2012, **23**, 2867.

27 S. C. Cox, P. Jamshidi, L. M. Grover, K. K. Mallick, *Mater. Sci. Eng. C,* 2014, **35**, 106.

28 K. Elayaraja, P. Rajesh, M. I. Ahymah Joshy, V. Sarath Chandra, R. V. Suganthi, J. Kennedy, P. K. Kulriya, I. Sulania, K. Asokan, D. Kanjilal, D. K. Avasthi, H. K. Varma and S. N. Kalkura, *Mater. Chem. Phys.,* 2012, **134**, 464.

29 C. Dong, A. Wu, S. Hao, J. Zou, Z. Liu, P. Zhong, A. Zhang, T. Xu, J. Chen, J. Xu, Q. Liu and Z. Zhou, *Surf. Coat. Technol.,* 2003, **163–164,** 620.

30 Q. F. Guan, H. Zou, G. T. Zou, A. M. Wu, S. Z. Hao, J. X. Zou, Y. Qin, C. Dong and Q. Y. Zhang, *Surf. Coat. Technol.,* 2005, **196**, 145.

31 D. I. Proskurovsky, V. P. Rotshtein, G. E. Ozur, A. B. Markov, D. S. Nazarov, V. A. Shulov, F. Yu, R. Ivanov and G. Buchheit, *J. Vac. Sci. Technol. A,* 1998, **16**, 2480.

32 D. Gopi, D. Rajeswari, S. Ramya, M. Sekar, R. Pramod, J. Dwivedi, L. Kavitha and R. Ramaseshan, *Appl. Surf. Sci.,* 2013, **286**, 83.

33 D. Gopi, A. Karthika, M. Sekar, L. Kavitha, R. Pramod and J. Dwivedi, *Mater. Lett.,* 2013, **105,** 216.

34 J. H. Lin, C. H. Chang, Y. S. Chen, and G. T. Lin, *Surf. Coat. Technol.,* 2006, **200**, 3665.

35 W. Xia, C. Lindahl, J. Lausmaa, P. Borchardt, A. Ballo, P Thomsen and H. Engqvist, *Acta Biomater.,* 2010, **6,** 1591.

36 D. Gopi, S. Ramya, D. Rajeswari and L. Kavitha, *Colloids Surf. B,* 2013, **107**, 130.

37 A. Kar, K. S. Raja and M. Misra, *Surf. Coat. Technol.,* 2006, **201,** 3723.

38 D. Gopi, V. C. A. Prakash and L. Kavitha, *Mater. Sci. Eng. C*, 2009, **29**, 955.

39 Y. Han, T. Fu, J. Lu and K. Xu, *J. Biomed. Mater. Res.,* 2001, **54**, 96.

40 D. Gopi, V. C. A. Prakash, L. Kavitha, S. Kannan, P. R. Bhalaji, E. Shinyjoy and J. M. F. Ferreira, *Corros. Sci.,* 2011, **53**, 2328.

41 M. Popa, E. Vasilescu, P. Drob, M.V. Popa, J. M. C. Moreno, C. Vasilescu and S. I. Drob, *J. Am. Ceram. Soc.,* 2012, **95**, 3807.

42 D. Gopi, J. Indira, and L. Kavitha, *J. Appl. Electrochem.,* 2013, **43**, 331.

43 Y. Y. Zhang, J. Tao, Y. -C. Pang, W. Wang and T. Wang, *Trans. Nonferrous Met. Soc. China,* 2006, **16**, 633.

44 Y. W. Gu, K. A. Khor, D. Pan, and P. Cheang, *Biomaterials,* 2004, **25**, 3177.

45 R. Drevet, H. Benhayounea, L. Worthama, S. Potirona, J. Dougladeb and D. L. Maquina, *Mater. Charact.,* 2010, **61**, 786.

46 ASTM standard F 1044–05. ASTM International, West Conshohocken, PA.

47 T. Kokubo and H. Takafama, *Biomaterials,* 2006, **27**, 2907.

48 D. Gopi, A. Karthika, S. Nithiya and L. Kavitha, *Mater. Chem. Phys.,* 2014, **144**, 75.

49 J. Guerra-Lopez, R. Pomes, C. O. D. Vedova, R. Vina, G. Punte, *J. Raman Spectrosc.* 2001, **32**, 255.

50 L. Oliveira, R. L. Reis and P. Li, *J. Biomed. Mater. Res. B Appl. Biomater.,* 2007, **83**, 258.

51 D. Guo, K. Xu, X. Zhao and Y. Han, *Biomaterials,* 2005, **26**, 4073.

52 R. N. Panda, H. Ming-Fa, R. J. Chung, T. S. Chin, *J. Appl. Phys.* 2001, **40**, 5030.

53 W. Xia, C. Lindahl, J. Lausma, P. Borchardt, A. Ballo, P. Thomsen, H. Engqvist, *Acta Biomater.* 2010, **6**, 1591.

54 J. Chen, Y. Song, D. Shan, E.H. Han, *Corros. Sci.* 2011, 53, 3281.

55 J. Li, L. Zhang, Y. Zuo, *Appl. Surf. Sci.* 2008, **254**, 2844.

56 A. Dey and A. K. Mukhopadhyay, *Int. J. Appl. Ceram. Technol.,* 2014, **11**, 65.

Figure Captions

Fig. 1. FT-IR spectra of M-HAP coating on (a) untreated Ti, (b) 500 keV HELCDEB treated Ti and (c) 700 keV HELCDEB treated Ti.

Fig. 2. Raman spectra showing (a) υ2 and υ4 signals and (b) υ1 and υ4 signals of M-HAP coating on (A, A') untreated Ti, (B, B') 500 keV HELCDEB treated Ti and (C, C') 700 keV HELCDEB treated Ti.

Fig. 3. XRD pattern of (a) pure Ti substrate (b) HAP coating on untreated Ti, and M-HAP coating on (c) untreated Ti, (d) 500 keV HELCDEB treated Ti and (e) 700 keV HELCDEB treated Ti.

Fig. 4. SEM images of (a) untreated Ti, (b) M-HAP coating on untreated Ti [Inset: magnified view], (c) cross-section image of (b), (d) 500 keV HELCDEB treated Ti (e) M-HAP coating on 500 keV HELCDEB treated Ti [Inset: magnified view] (f) cross-section image of (d), (g) 700 keV HELCDEB treated Ti (h) M-HAP coating on 700 keV HELCDEB treated Ti [Inset: magnified view], (i) cross-section image of (h), and (j) EDAX spectrum for the M-HAP coating on 700 keV HELCDEB treated Ti.

Fig. 5. XPS survey spectrum of M-HAP coating on 700 keV HELCDEB treated Ti.

Fig. 6. Contact angle measurement of (a) untreated Ti, (b) 500 keV HELCDEB treated Ti and (c) 700 keV HELCDEB treated Ti.

Fig. 7. Adhesion strength measurement of M-HAP coating on (a) untreated Ti, (b) 500 keV HELCDEB treated Ti and (c) 700 keV HELCDEB treated Ti.

Fig. 8. Vickers microhardness measurement of M-HAP coating on (a) untreated Ti, (b) 500 keV HELCDEB treated Ti and (c) 700 keV HELCDEB treated Ti.

Fig. 9. Potentiodynamic polarization curves of (a) untreated Ti, (b) 500 keV HELCDEB treated Ti (c) 700 keV HELCDEB treated Ti, and M-HAP coating on (d) untreated Ti, (e) 500 keV HELCDEB treated Ti (f) 700 keV HELCDEB treated Ti.

Fig. 10. ICP AES analysis of M-HAP coating on 700 keV HELCDEB treated Ti at different immersion time.

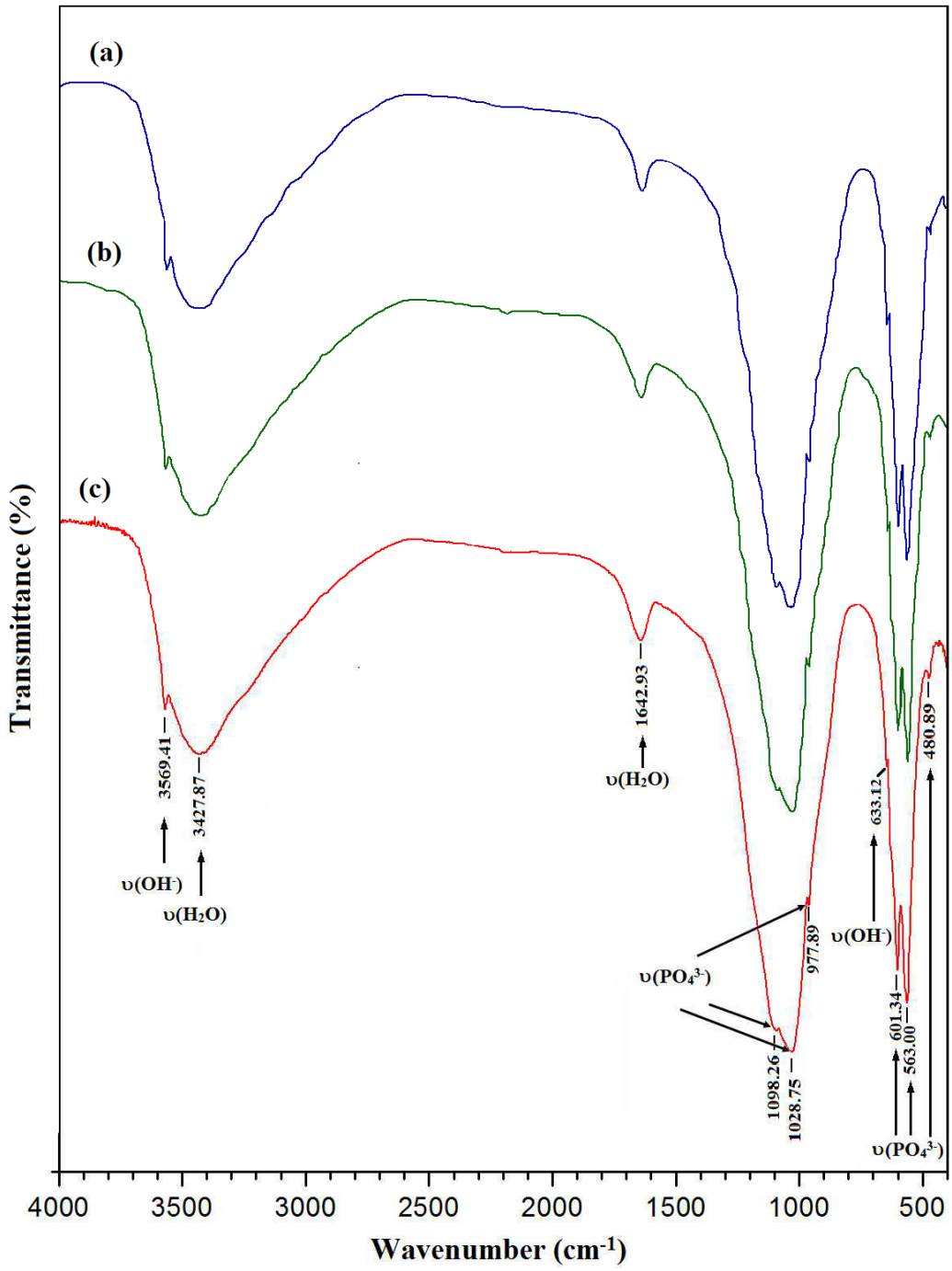

Fig. 1. FT-IR spectra of M-HAP coating on (a) untreated Ti, (b) 500 keV HELCDEB treated Ti and (c) 700 keV HELCDEB treated Ti.

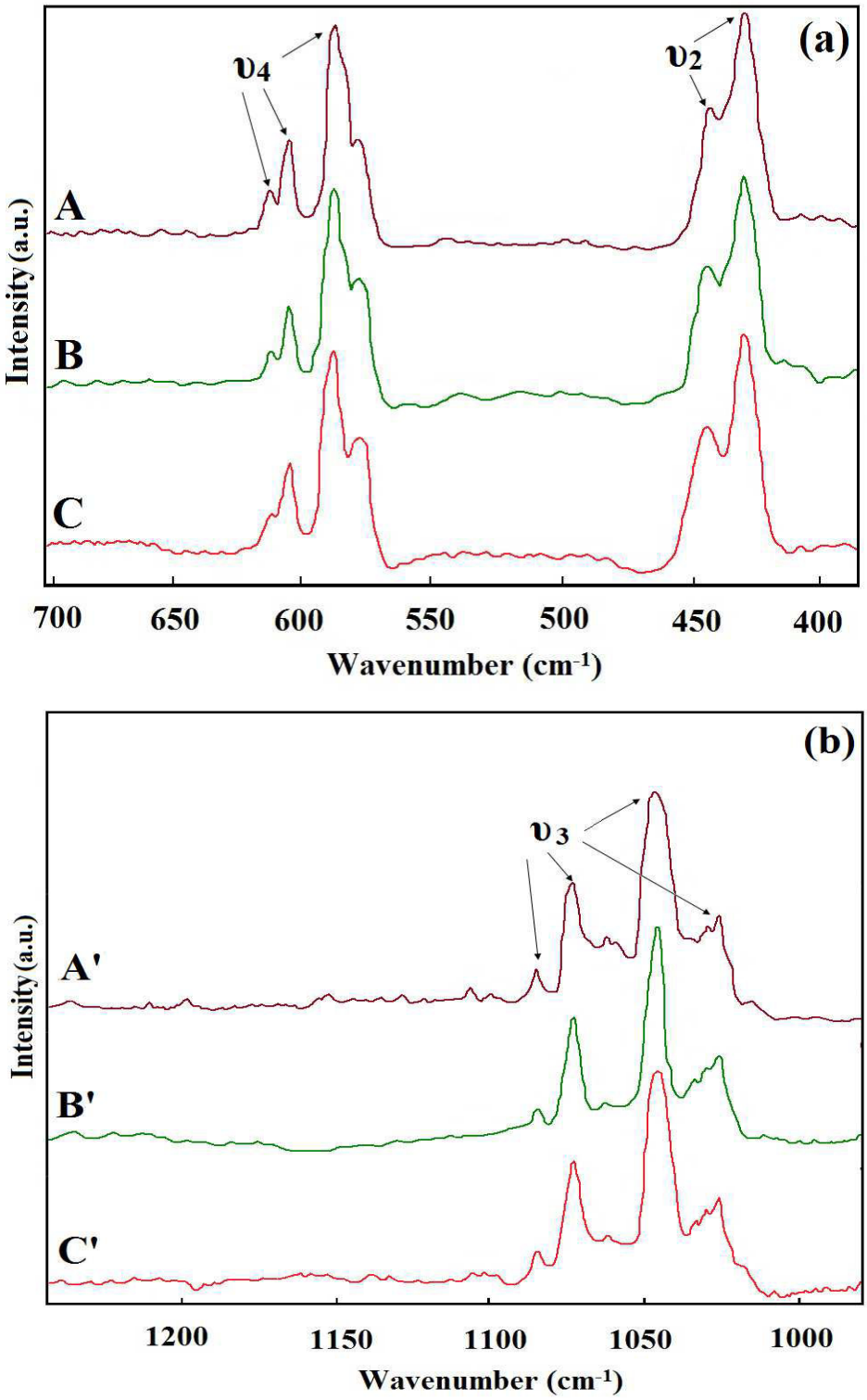

Fig. 2. Raman spectra showing (a) υ_2 and υ_4 signals and (b) υ_3 signals of M-HAP coating on (A, A') untreated Ti, (B, B') 500 keV HELCDEB treated Ti and (C, C') 700 keV HELCDEB treated Ti.

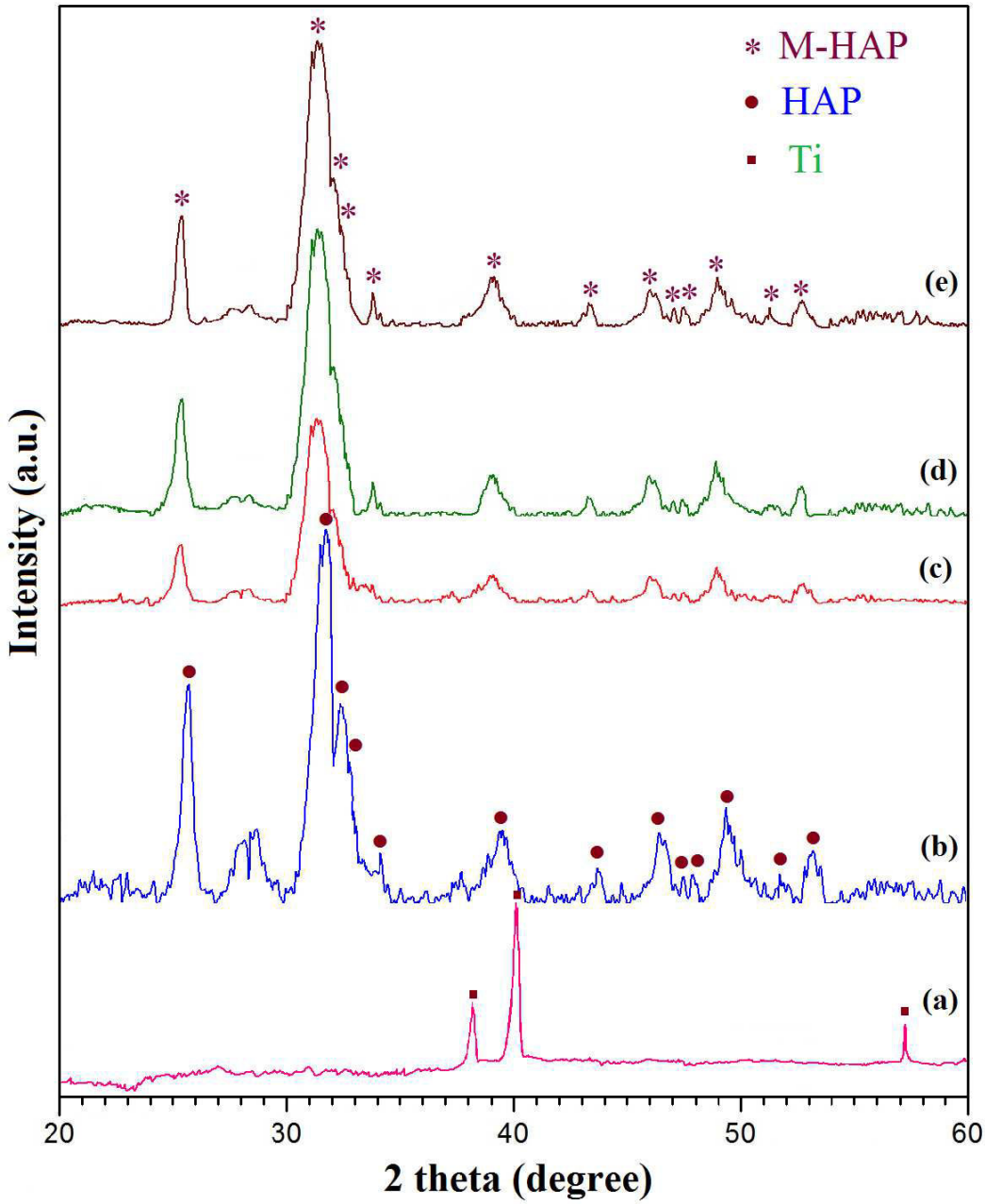

Fig. 3. XRD pattern of (a) pure Ti substrate (b) HAP coating on untreated Ti, M-HAP coating on (c) untreated Ti, (d) 500 keV HELCDEB treated Ti and (e) 700 keV HELCDEB treated Ti.

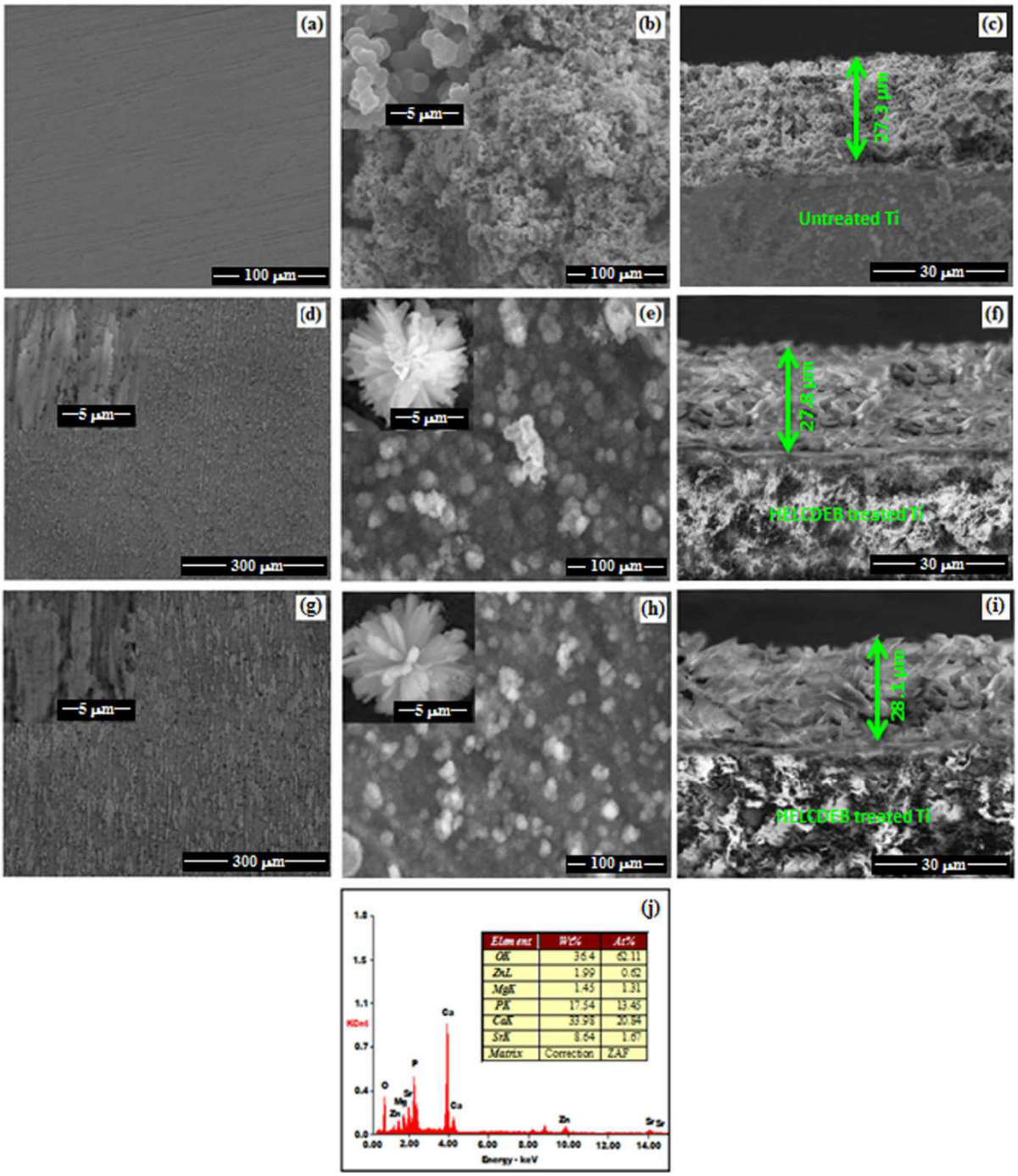

Fig. 4. SEM images of (a) untreated Ti, (b) M-HAP coating on untreated Ti [Inset: magnified view], (c) cross-section image of (b), (d) 500 keV HELCDEB treated Ti (e) M-HAP coating on 500 keV HELCDEB treated Ti [Inset: magnified view] (f) cross-section image of (d), (g) 700 keV HELCDEB treated Ti (h) M-HAP coating on 700 keV HELCDEB treated Ti [Inset: magnified view], (i) cross-section image of (h), and (j) EDAX spectrum for the M-HAP coating on 700 keV HELCDEB treated Ti

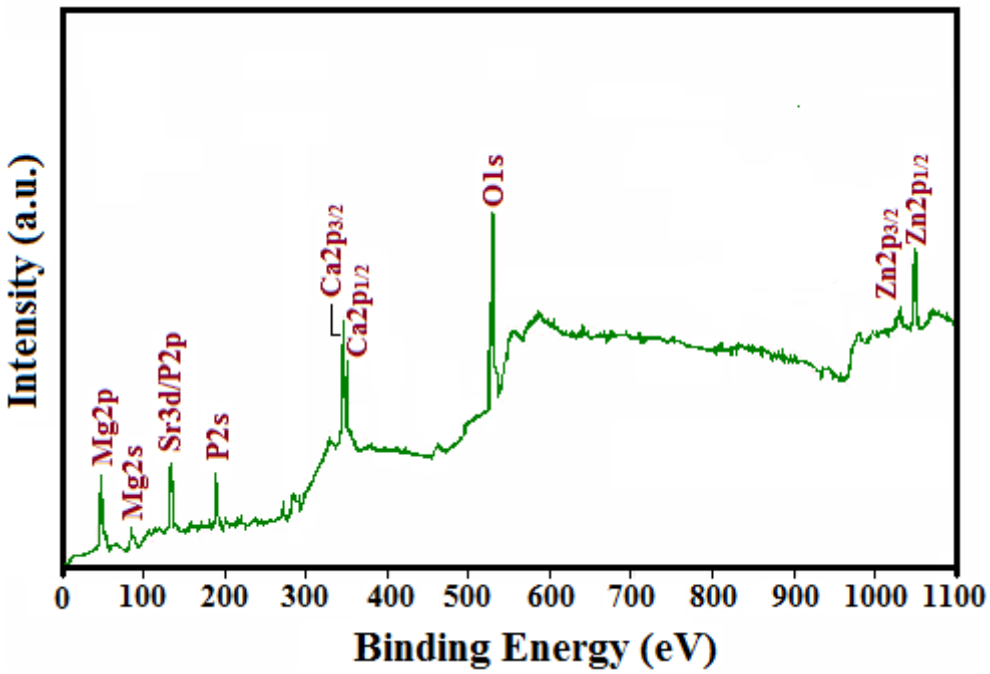

Fig. 5. XPS survey spectrum of M-HAP coating on 700 keV HELCDEB treated Ti.

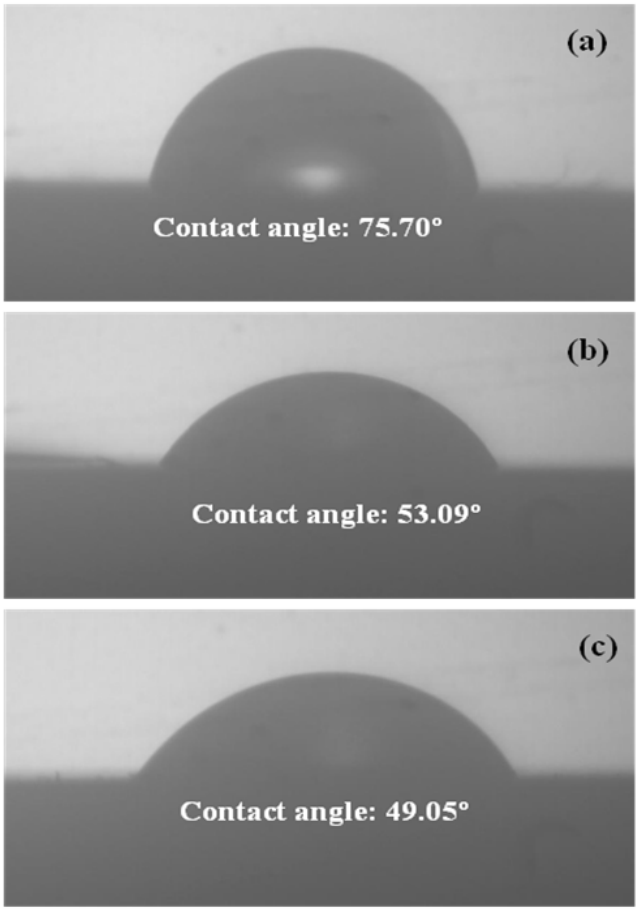

Fig. 6. Contact angle measurement of (a) untreated Ti, (b) 500 keV HELCDEB treated Ti and (c) 700 keV HELCDEB treated Ti.

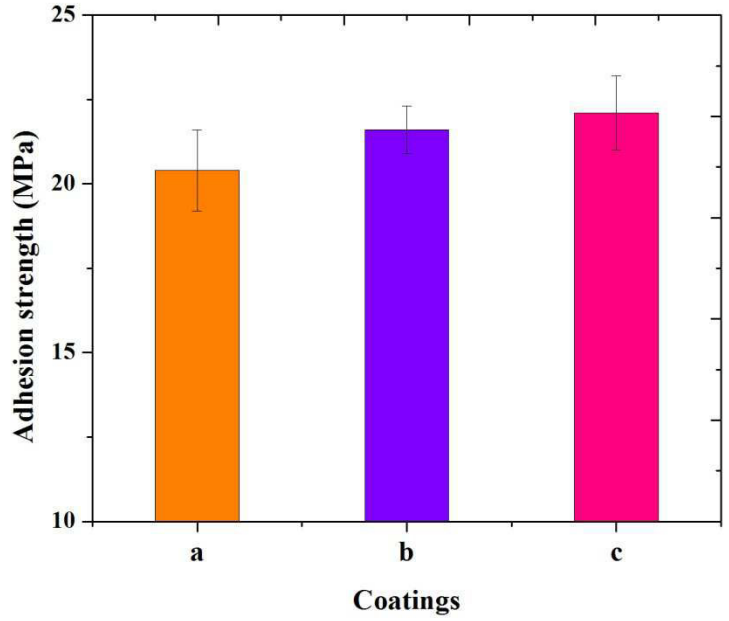

Fig. 7. Adhesion strength measurement of M-HAP coating on (a) untreated Ti, (b) 500 keV HELCDEB treated Ti and (c) 700 keV HELCDEB treated Ti.

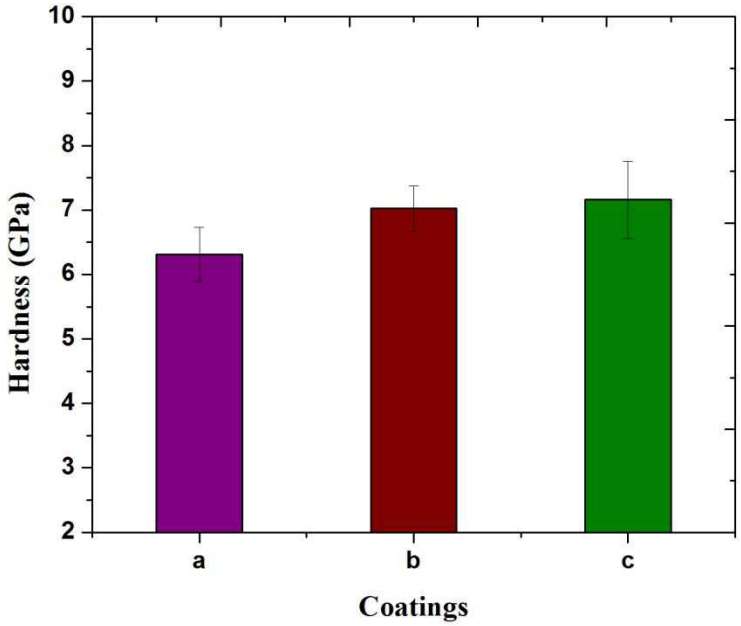

Fig. 8. Vickers microhardness measurement of M-HAP coating on (a) untreated Ti, (b) 500 keV HELCDEB treated Ti and (c) 700 keV HELCDEB treated Ti.

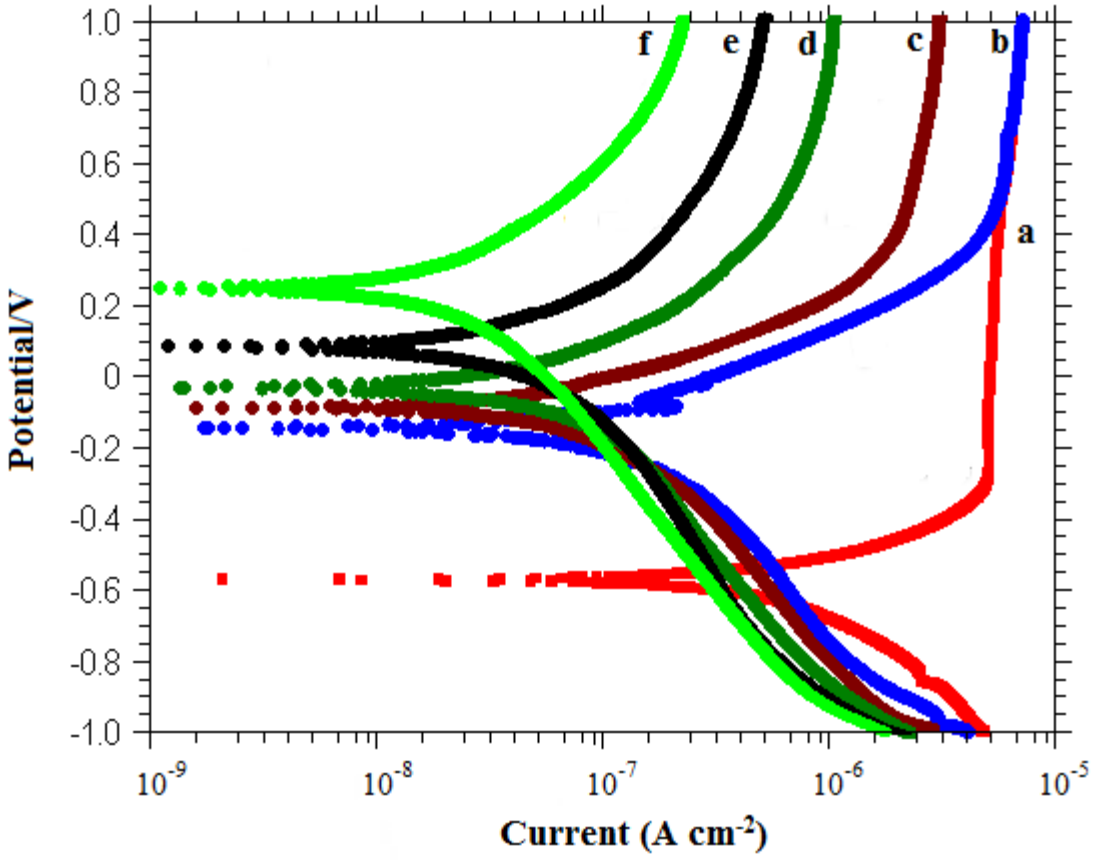

Fig. 9. Potentiodynamic polarization curves of (a) untreated Ti, (b) 500 keV HELCDEB treated Ti (c) 700 keV HELCDEB treated Ti, and M-HAP coating on (d) untreated Ti, (e) 500 keV HELCDEB treated Ti (f) 700 keV HELCDEB treated Ti.

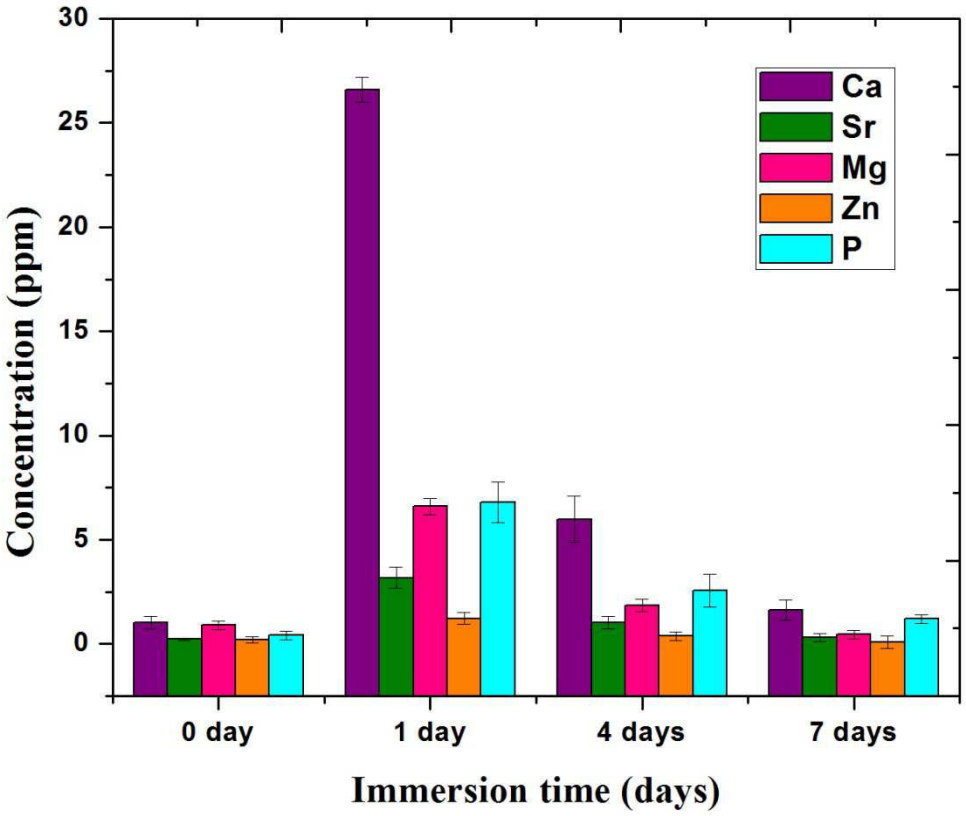

Fig. 10. ICP AES analysis of M-HAP coating on 700 keV HELCDEB treated Ti at different immersion time.